journal of the mechanical behavior of biomedical materials 151 (2024) 106408

Contents lists available at ScienceDirect

Journal of the Mechanical Behavior of Biomedical Materials

journal homepage: www.elsevier.com/locate/jmbbm

Remineralizing effects of hydroxypropyl methylcellulose film-loaded amorphous calcium phosphate nanoprecursors on enamel artificial caries lesions

Zhixin Zhang [a,b,*,1], Zihan Cui [a,1], Jianping Zhang [c], Haiyan Zheng [a], Zihuai Zhou [a], Zhifang Wu [a], Zhe Wang [a,**], Baiping Fu [a,***]

[a] Stomatology Hospital, School of Stomatology, Zhejiang University School of Medicine, Zhejiang Provincial Clinical Research Center for Oral Diseases, Key Laboratory of Oral Biomedical Research of Zhejiang Province, Cancer Center of Zhejiang University, Engineering Research Center of Oral Biomaterials and Devices of Zhejiang Province, Hangzhou, 310000, China

[b] Department of Stomatology, Quanzhou First Hospital Affiliated to Fujian Medical University, Quanzhou, 362000, Fujian, China

[c] Department of Orthopaedics, The 909th Hospital, School of Medicine, Xiamen University, Zhangzhou, 363000, Fujian, China

ARTICLE INFO

Keywords:
Enamel caries
Remineralization
Calcium phosphate nanoprecursors
Nanoindentation

ABSTRACT

Objectives: This study was to investigate hydroxypropyl methylcellulose (HPMC) film as a carrier for amorphous fluorinated calcium phosphate (AFCP) nanoprecursors to continuously deliver biomimetic remineralization of enamel artificial caries lesions (ACL).

Materials and methods: The AFCP/HPMC films were comprised of 25 wt% AFCP nanoparticles and 75 wt% HPMC. They were characterized by transmission electron microscopy (TEM), Fourier transform infrared spectroscopy (FTIR), X-ray diffraction (XRD), X-ray photoelectron spectroscopy (XPS), and biocompatibility tests. Forty enamel ACL were prepared and randomly divided into four groups (n = 10): The enamel surfaces were covered with a pure HPMC film, Tooth Mousse Plus (contains 10% CPP-ACP and 0.2% NaF), and AFCP/HPMC film, or without any things (serving as negative control). Subsequently, all samples were alternatively kept in artificial saliva and a modified pH-cycling before they were characterized by Micro-CT, scanning electron microscopy (SEM), energy-dispersive X-ray spectroscopy (EDX), attenuated total reflectance (ATR)-FTIR, XRD, and nanoindentation.

Results: After the enamel ACL was challenged by pH cycling, Tooth Mousse Plus and AFCP/HPMC film groups exhibited less lesion depth and mineral loss than the negative control and pure HPMC film groups. Additionally, the AFCP/HPMC film group revealed a highest remineralization rate of 55.34 ± 3.10 % among the all groups ($p < 0.001$). The SEM findings showed that the enamel ACL were densely deposited with minerals in the AFCP/HPMC film group, and the EDX results suggested a higher content of fluorine in the remineralized tissues. In particular, the AFCP/HPMC film group exhibited the best nanomechanical performance after 2 weeks of pH cycling ($p < 0.05$), with the hardness (H) restored from 0.29 ± 0.19 to 2.69 ± 0.70 GPa, and elastic modulus (Er) restored from 10.77 ± 5.30 to 68.83 ± 12.72 GPa.

Conclusion: The AFCP/HPMC film might be used as a promising strategy for arresting or reversing incipient enamel caries lesions.

* Corresponding author. Stomatology Hospital, School of Stomatology, Zhejiang University School of Medicine, Zhejiang Provincial Clinical Research Center for Oral Diseases, Key Laboratory of Oral Biomedical Research of Zhejiang Province, Cancer Center of Zhejiang University, Engineering Research Center of Oral Biomaterials and Devices of Zhejiang Province, Hangzhou, 310000, China.

** Corresponding author.

*** Corresponding author.

E-mail addresses: 1934800300@qq.com (Z. Zhang), 7319012@zju.edu.cn (Z. Wang), fbp@zju.edu.cn (B. Fu).

[1] Authors contributed equally.

https://doi.org/10.1016/j.jmbbm.2024.106408
Received 23 November 2023; Received in revised form 12 January 2024; Accepted 15 January 2024
Available online 17 January 2024

1. Introduction

Dental caries is a serious health problem that affects 60–90% of children and almost 100% of adults worldwide (Balhaddad et al., 2018). Tooth caries typically begins with the demineralization of enamel and then gradually progresses to the underlying dentin and pulp, causing a cavitated lesion or even tooth loss (Pitts et al., 2017). Although mature enamel is highly mineralized and provides an insulating barrier that protects the teeth from daily mechanical wear, acidic erosion, or bacterial attack (Lacruz et al., 2017; Sa et al., 2014); it lacks of the ability to self-repair or remodel once damaged (Ruan and Moradian-Oldak, 2015). For this reason, the early prevention and treatment of dental caries are of great important in dentistry. Caries prevention primarily focuses on demineralization of tooth hard tissues and oral microflora, while treatment of enamel incipient caries is also great important.

Conventional treatment for dental caries lesions involves artificial filling materials (e.g. glass ionomer cement and composite resins) in a cavitation where the demineralized tooth hard tissues have to be mechanically removed (Bayne et al., 2019; Cramer et al., 2011). Nevertheless, the clinical procedure is not optimal for early enamel carious lesions that could be restored by biomimetic mineralization technique (Wang et al., 2021; Fang et al., 2021). In addition, the components, microstructures, and physicochemical properties of dental restorative materials are much different from nature tooth hard tissues (Stewart and Finer, 2019; Gauthier et al., 2021), and the weakness at interface of the artificial dental material-tooth hard tissues could result in secondary caries (Gauthier et al., 2021; Demarco et al., 2012). Thus, the induction of self-healing and regeneration prior to cavity formation has become a daunting challenge in clinical dentistry (Balhaddad et al., 2018; El Gezawi et al., 2019).

It is well established that dental caries is a chronic, progressive disease, that involves an imbalance of de- and remineralization process (Abou Neel et al., 2016). In the early stages of caries, this balance can be reversed and the lesion can be restored by using a remineralizing agent. Topical fluoride treatment remains a key element in caries management (Benson et al., 2019). Fluorine (F^-) produces tremendous biological benefits in synergy with calcium (Ca^{2+}) and phosphate (PO_4^{3-}) in saliva, conferring better anti-acid and antimicrobial effects on the enamel. However, the absence of or low concentration of mineral ions, such as Ca^{2+} and PO_4^{3-} ions, can make it difficult to effectively regenerate hydroxyapatite (HAP) crystals on the surface of demineralized enamel (Lippert and Juthani, 2015; Philip, 2019; He et al., 2022). Furthermore, fluoride treatment alone tends to form a hypermineralized layer on the enamel surface, which would block the movement of mineral ions into enamel subsurface so as to hinder remineralization of deeper lesions (Lyaruu et al., 2014).

Recently, biomineralization technology has provided a strategy for reconstructing the tooth hard tissues. In particular, the ability to release significant amount of Ca^{2+} and PO_4^{3-} ions has made the amorphous calcium phosphate (ACP) being highly desired for remineralization of tooth hard tissues (Combes and Rey, 2010). As a precursor (transient) of biogenic HAP for bone and teeth, ACP has excellent biological activity (DeRocher et al., 2020; Eanes et al., 1973). The application of ACP nanoparticles has become a frequently used biomimetic mineralization strategy, due to its high reactivity and excellent ability to adhere and penetrate into enamel and dentin caries lesions (Combes and Rey, 2010; Dorozhkin, 2010). However, the ACP is not thermodynamically stable under humid conditions and can spontaneously convert to crystalline apatite (Eanes et al., 1973; Rabadjieva et al., 2010). Casein phosphopeptide (CPP) (Cochrane et al., 2008), carboxymethyl chitosan (CMC) (Xiao et al., 2017), polyaspartic acid (PASP) (Cantaert et al., 2013), and polyacrylate acid (PAA) (Li et al., 2021), have already proven effective to simulate the role of non-collagen analogues (NCPs) to stabilize the amorphous phase of ACP, and mediate the crystalline phase transformation of ACP (L. Yu et al., 2018). Harnessing this knowledge, various strategies that based on ACP nanoprecursors have been applied to mouthwash (Reynolds et al., 2003), toothpaste (Shen et al., 2018), and dental composite resins (Zhang et al., 2016), so as to induce the biomimetic remineralization of demineralized enamel. However, the materials in liquid and paste state are not favorable for remineralizing process, due to their short duration of action. Additionally, the insoluble drug delivery vehicles would constrain the release and diffusion of loaded ACP particles. Therefore, the development of new drug forms that provide sustained release of mineralizing agents is compelling.

Nowadays, polymeric excipients are widely applied because of their solubilization property (Baghel et al., 2016), and they also can act as a crystallization inhibitor to modulate the drug release rate and maintain drug supersaturation (Tran et al., 2011). Thereinto, hydroxypropyl methylcellulose (HPMC) as a hydrophilic cellulose derivative, with ether-linked methoxy and hydroxypropyl side groups, has been widely used as oral controlled drug delivery system (Siepmann and Peppas, 2001). HPMC can control the rate of drug release via forming a gel layer on the matrix surface upon water absorption. In our previous study, HPMC was carried with solid amorphous fluorinated calcium phosphate (AFCP) nanoparticles to form a AFCP/HPMC film, and this film could inhibit the formation of enamel white spot lesions (WSLs) (Zhang et al., 2021). However, its remineralizing efficacy has not been explored. Thus, the objective of this study was to assess the therapeutic effects of AFCP/HPMC film on enamel ACL. The null hypotheses were that AFCP/HPMC film neither could promote remineralization of enamel ACL, nor restore mechanical properties of enamel ACL.

2. Materials and methods

2.1. Synthesis of AFCP/HPMC film

The AFCP nanoparticles and AFCP/HPMC film were synthesized as previously described (Zhang et al., 2021). Firstly, the polyaspartic acid stabilized-calcium (PASP-Ca) solution containing 10 mM $CaCl_2$ and 480 μg/mL PASP, and the phosphate solution containing 6 mM Na_2HPO_4 and 110 ppm NaF, were separately prepared with deionized water. Next, both solutions were mixed at equal volumes with their pH simultaneously titrated to 9.5, under the magnetic stirring. Subsequently, the precipitates were collected by centrifugation before they were washed with deionized water and ethanol in turn, dried in an oven at 70 °C for 2 h. The AFCP nanoparticles were obtained by grinding the dried precipitates. Finally, 150 mg HPMC powder was fully swelled in 70% (v/v) ethanol to prepare a HPMC gel and then mixed with 50 mg AFCP nanoparticles, the final mixture was poured on glass plate and oven-dried to form an AFCP/HPMC film (thickness 0.1 mm, mass 0.33 mg/mm^2). Similarly, the pure HPMC film was prepared without addition of AFCP nanoparticles. The AFCP nanoparticles were analyzed by transmission electron microscopy (TEM, JEOL, Tokyo, Japan), Fourier transform infrared spectroscopy (FTIR, Nicolet iS10, Thermo Scientific), X-ray powder diffraction (XRD, D/max-2550pc, Rigaku) and X-ray photoelectron spectroscopy (XPS, Thermo Scientific, K-alpha). The biocompatibility tests of AFCP/HPMC film are described in the Supplementary Information (SI) for detailed methods.

2.2. Preparation of enamel artificial caries lesions (ACL)

Thirty healthy human premolars were used in this study that was approved by the Ethics Committee of the Hospital of Stomatology, Zhejiang University (No. 2019–05). The buccal and lingual surfaces of tooth enamel were cut into 4 mm × 4 mm × 1.5 mm blocks using a low-speed saw (Isomet, Buehler, Lake Bluff IL, USA) under the copious water cooling. Then, the outer enamel surfaces were polished with ascending grits (P600, P1200, P2500, P4000) of silicon carbide (SiC) papers, and ultrasonicated in deionized water for 5 min to remove any debris. After that, the finished surfaces were covered with acid-resistant nail varnish to expose a working window of 3 mm × 3 mm.

The finished enamel slices were immersed in a demineralization

solution that consisted of 50 mM acetic acid, 2.2 mM $CaCl_2$, 2.2 mM KH_2PO_4, 0.02% Na_3N and 0.02 ppm NaF (O.Y. Yu et al., 2018). The pH of the buffer solution was titrated to 4.5 with 1 M NaOH. During the acidic challenge, each slice was individually immersed in 5 mL of the freshly prepared demineralization solution and incubated at 25 °C for 6 days to create enamel ACL. The samples were then scanned with Micro-CT to confirm enamel demineralization.

2.3. In vitro remineralization experiments

Forty enamel ACL samples were randomly assigned to 4 groups (n = 10) according to different treatment strategies. The enamel surface was covered without any things (serving as negative control; Group1), or covered with pure HPMC film of 3 mm × 3 mm × 0.1 mm (Group 2), covered with Tooth Mousse Plus (Group 3), and covered with AFCP/HPMC film of 3 mm × 3 mm × 0.1 mm (Group 4). They were immersed in artificial saliva for 8 h. After that, they were subjected to acid challenge in demineralization solution for 1 h and then incubated in artificial saliva for another 15 h. Each sample was rinsed immediately with deionized water to remove loosely attached molecules and blot-dried at each stage. The re-, de- and remineralization process mentioned above was repeated for 2 weeks. All samples were incubated at room temperature without stirring. The artificial saliva (pH 7.0, adjusted with 1 M NaOH) containing 1.5 mM $CaCl_2$, 0.9 mM KH_2PO_4, 130 mM KCl, 1.0 mM NaN_3, and 20 mM HEPES (Yang et al., 2014). Following pH cycling, the samples were collected for the assessment of remineralization. The experimental procedure is schematically shown in Fig. 1.

2.4. Characterizations

2.4.1. Evaluation of lesion depth and mineral content

To assess the changes of mineral content and lesion depth, each enamel slice at baseline, after 6 days of demineralization, and after 2 weeks of remineralization was repeatedly scanned with a Micro-CT imaging system (Milabs, Netherlands). Scanning was performed with an accurate scan mode at 50 kV and 210 mA. The projection images were taken with the exposure time of 75 ms, and with the samples rotated 360° at step angle of 0.25°. Each sample was re-scanned with the same acquisition and reconstruction parameters during different time points. After scanning, each sample was 3D reconstructed by using Milabs software, and then further processed with Imalytics Preclinical 2.1 (version 2.1.8.9) to obtain a 3D image stack. The virtual serial sections of each sample were saved and subjected to visualization and quantitative measurements. The representative 2D images of each sample were analyzed with Image J software (National Institutes of Health, USA) to produce an overall greyscale value profile within a standardized region of interest (ROI). The assessment was conducted in the same area, and a representative zone (depth of 500 μm) of the stacked image was plotted. The lesion depth (LD) and mineral loss were calculated from the relative greyscale value profile. The LD was recorded as the depth of the region where the greyscale value reached the baseline. The mineral loss (ΔZ) was calculated by integrating the area under the greyscale value profile on each sample at baseline and after demineralization. The remineralization rate of each sample was calculated using the following equation: remineralization rate (R) = $(\Delta Z - \Delta Z_a)/(\Delta Z)$, where ΔZ_a is the data after remineralization.

2.4.2. Evaluation of microstructures

After dehydration in a series of ethanol (50%, 70%, 90%, 95%, 100%), samples were air dried and gold-sputtered. The morphology of enamel surface and cross-section were investigated by SEM using an accelerating voltage of 3 kV, and the elemental composition of enamel surfaces was measured by EDX attached to a field-emission scanning electron microscope at 15 kV (Zeiss Gemini SEM 300, Oberkochen, Germany).

2.4.3. Evaluation of chemical characteristics

The chemical functional groups of the polished, de- and remineralized enamel surfaces were tested by ATR-FTIR, in absorbance mode over a 400–4000 cm^{-1} range at a resolution of 4 cm^{-1} (Sun et al., 2011). The compositions and structures of the polished, de- and remineralized enamel surfaces were determined by X-ray diffractometer (D/max2500, Rigaku) at 40 kV and 200 mA, using Cu-Kα radiation. Thin-film XRD patterns were recorded in the 2θ range of 4°–60° with a scan rate of 0.02°/s. The data were further processed with OriginPro 9.1 software (OriginLab Corporation, USA) and compared with standard diffraction

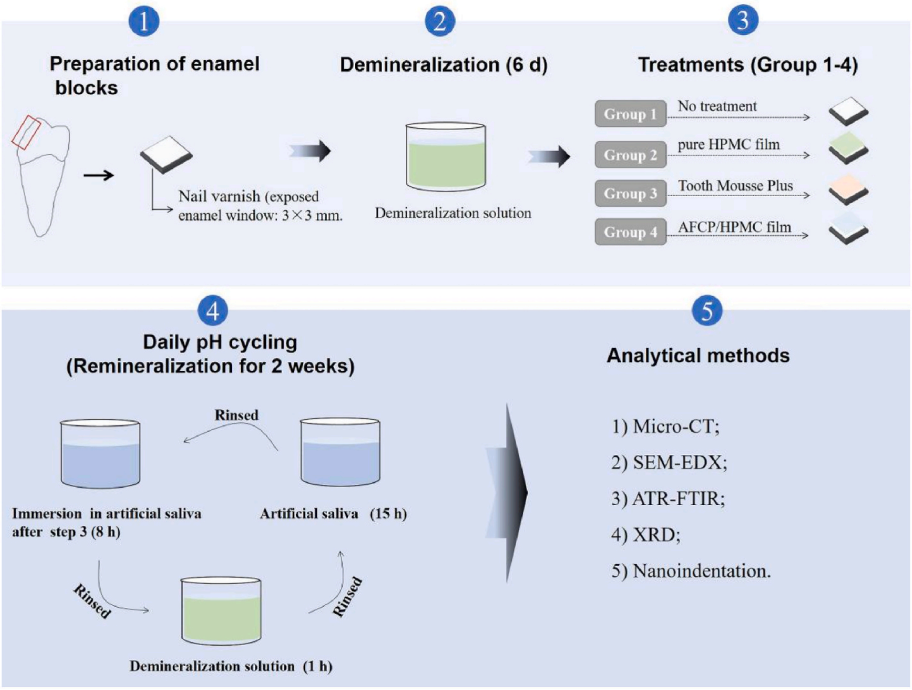

Fig. 1. Schematic diagram of the treatment process.

peak card of hydroxyapatite (JCPDS No. 09–0432) (Fang et al., 2021).

2.4.4. Evaluation of mechanical properties

The nanohardness and elastic modulus of the samples were measured using a nanoindenter (G200; Agilent Technologies, USA) equipped with a Berkovich probe. The maximum force applied was 15 mN with the loading time maintained at 5 s. Five points per sample were determined. During the test, the loading force and indentation depth of the samples were continuously measured to obtain load-displacement curves, based on which the nanohardness (H) and elastic modulus (Er) were calculated (Oliver and Pharr, 2004).

2.5. Statistical analysis

The data were processed and analyzed statistically by SPSS software, version 24.0 (IBM Corp, Armonk, USA). Data normality and homogeneity of variance were determined using Shapiro-Wilk and Levene's test, respectively; after that, a one-way ANOVA with Tukey's HSD post hoc test were conducted. Any difference was deemed statistically significant when p value was set <0.05.

3. Results

3.1. Characteristics of AFCP nanoparticles and AFCP/HPMC film

Fig. 2 reveals the characteristics of the AFCP particles in this study. The TEM image indicates the size of the AFCP particles to be approximately 30–50 nm (Fig. 2A). The FTIR spectrum reveals two wide bands typical for phosphate stretching (υ3) at 1050 cm^{-1} and phosphate bending (υ4) at 560 cm^{-1} (Fig. 2B). The XRD pattern shows a broad peak at $2\theta = 30°$ (Fig. 2C). The XPS spectra confirm that calcium, phosphate, fluorine, oxygen, and carbon are present in the AFCP nanoparticles (Fig. 2D). The cytotoxicity and oral mucosa irritation assays showed that AFCP/HPMC film has good biocompability (Fig. S1).

3.2. Micro-CT analysis

The representative micro-CT images from each group are displayed in Fig. 3. After 6 days of demineralization, typical subsurface lesions showed a visible carious lesion with decreased grayscale values in any of the four groups (before pH cycling) (Fig. 3a_1,c_1,e_1,g_1). After 2 weeks of remineralization, the grayscale value in the lesions revealed almost no changes in Group 1 and 2 compared with the baseline condition (Fig. 3a_2, c_2). Treatment with Tooth Mousse Plus (Group 3) did not significantly improve the lesion depth despite partial increases in the inhomogeneous grayscale values (Fig. 3e_2). As a result of remineralization treatment with AFCP/HPMC film (Group 4), computed tomography (CT) intensity was significantly increased in the demineralized lesion area and the distribution of grayscale values was more homogeneous (Fig. 3g_2). The relative gray values profiles in representative samples from each group are illustrated in Fig. 3b, d, f, h. After 2 weeks of remineralization, the relative gray values in the Group 1, 2 and 3 was only a slight increase, whereas Group 4 led to the evident changes in the gray value profiles. Additionally, the quantitative results of the lesion depth and mineral loss in enamel samples of each group further verified that the AFCP/HPMC film exhibited better function in the remineralization of enamel ACL, with a remineralization rate of 55.34 ± 3.10% (Fig. 3i-k).

3.3. SEM observation with EDX

The micrographs of enamel surfaces are presented in Fig. 4. Before demineralization, the enamel surface was smooth and flat, with polishing scratches visible (Fig. 4a_1, a_2); the cross-section showed an intact structure of enamel rods and inter-rods, within them, the crystals arranged in parallel and packed closely into bundles (Fig. 4a_3, a_4). After 6 days of acid demineralization, the enamel surface showed the characteristic of 'fish scales' surface with micro-cavities (Fig. 4b_1, b_2); the cross-section exhibited a porous and disordered micro-structure, with partial disappearance of inter-rods and discontinuous broken of crystals (Fig. 4b_3, b_4). The typical morphology of the acid-etched enamel surface

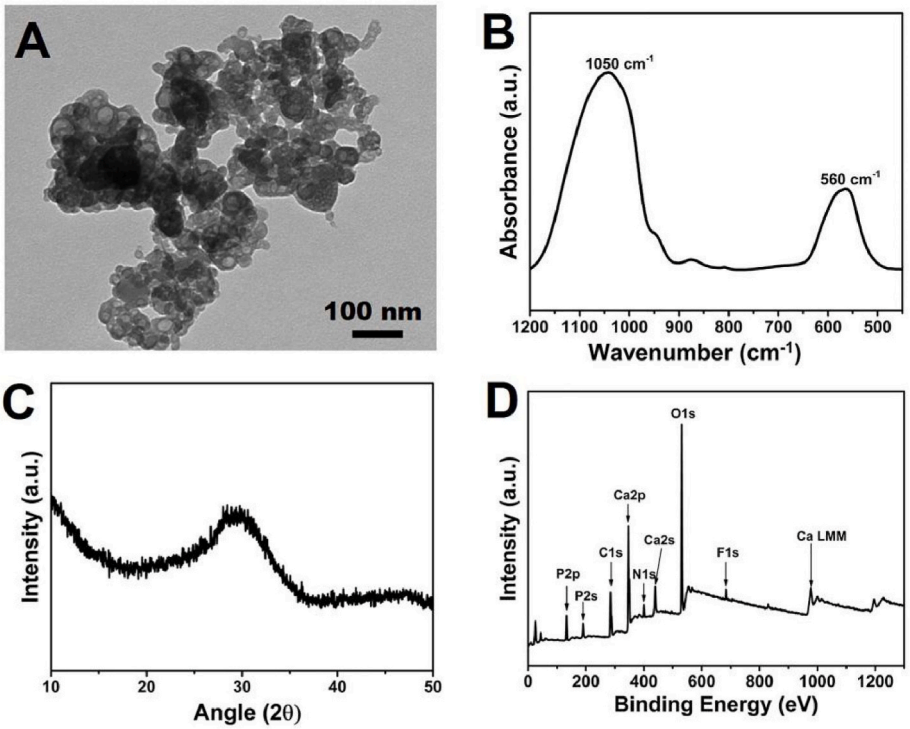

Fig. 2. Characteristics of AFCP nanoparticles. (A) TEM image. (B) FTIR spectrum. (C) XRD spectrum. (D) Wide-scan XPS spectrum.

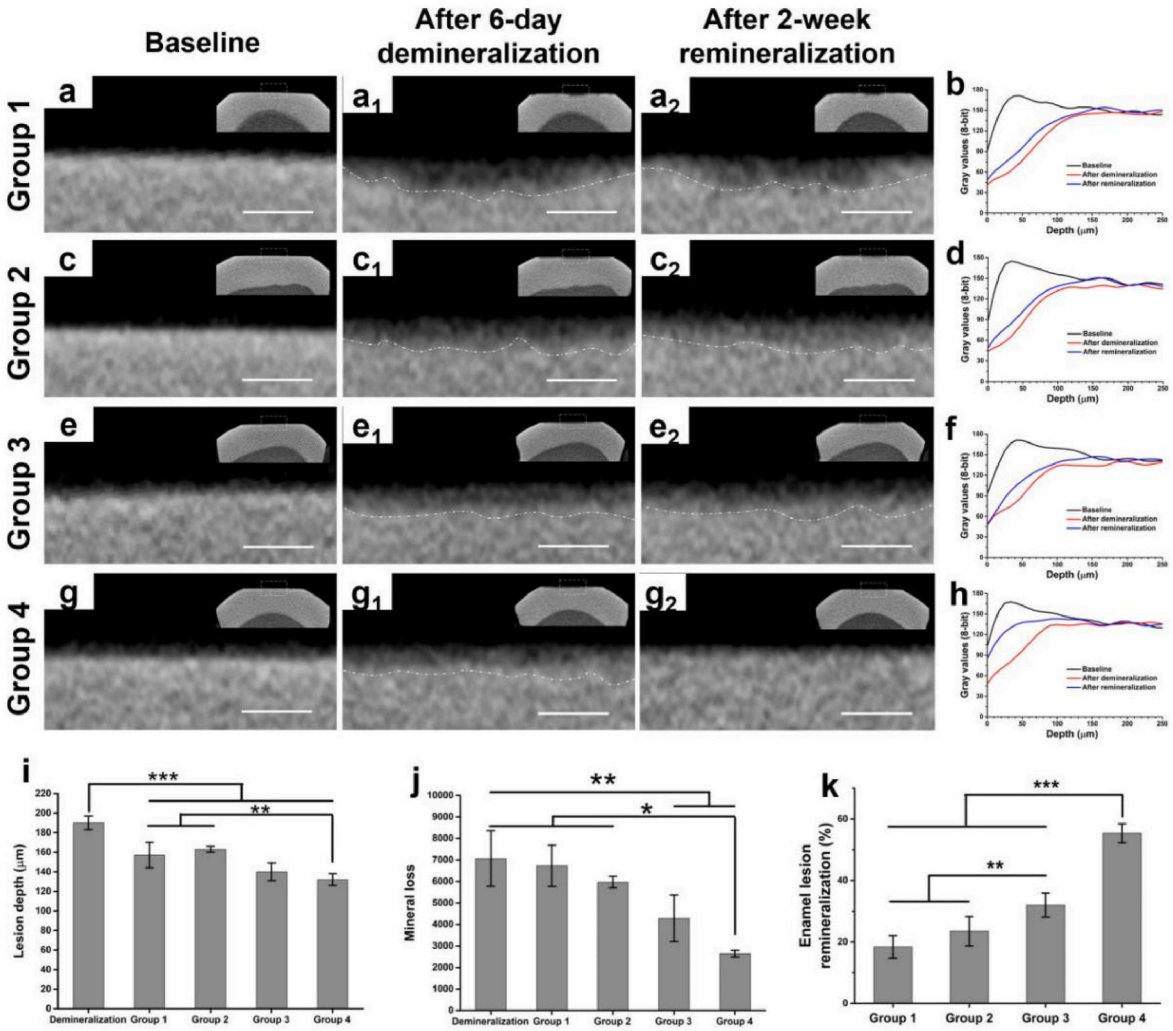

Fig. 3. AFCP/HPMC film induced remineralization of enamel carious lesions in vitro. (a–h) Representative micro-CT images (cross-sectional slices) and the relative gray value profiles for each group: Baseline (a, c, e, g); after 6-day demineralization (a_1, c_1, e_1, g_1); after 2-week remineralization (a_2, c_2, e_2, g_2); relative gray value profiles (b, d, f, h). Scale bar: 250 μm. (i) Lesion depth of enamel slices after 2-week remineralization in each group. (j) Mineral loss of enamel slices after 2-week remineralization in each group. (k) Enamel lesion remineralization rate after 2-week remineralization. The remineralization rate of samples in each group was calculated by the following formulation: remineralization rate = $(\Delta Z - \Delta Z_a)/(\Delta Z)$, where ΔZ denotes data of mineral loss before pH cycling and ΔZ_a after pH cycling. mean ± SD; *p < 0.05, **p < 0.01, ***p < 0.001.

was still clearly visible after 2-week remineralization treatments in Group 1 and 2, the micro-structure of the enamel prisms was still clearly exposed (Fig. 4$c_{1\text{-}4}$; $d_{1\text{-}4}$). In Group 3, the morphology of demineralized enamel became less pronounced and the interstitial space among crystals reduced (Fig. 4e_1, e_2); the cross-section showed that the damaged enamel was incompletely repaired, with the new minerals partially deposited and the crystal gaps remained (Fig. 4e_3, e_4). In contrast, the Group 4 showed a dense layer of disorder mineral crystals deposited on the enamel surface and the previously eroded structures had completely disappeared (Fig. 4f_1, f_2); the cross-section micrograph showed a well repaired enamel structures with the exposed crystal spaces being tightly wrapped by new minerals (Fig. 4f_3, f_4). The EDX results showed that there was no significant difference of Ca/P atomic ratio in different enamel surfaces, whereas, the Group 4 had a higher Ca/F atomic ratio than the other groups (Fig. S2).

3.4. ATR-FTIR and XRD analyses

The chemical functional groups of different enamel surfaces were investigated by ATR-FTIR. As shown in Fig. 5a, the characteristic bands at 981 - 1011 cm^{-1} and 953 - 959 cm^{-1} are corresponding to the asymmetric (υ3) and symmetric (υ1) stretching vibration of PO_4^{3-}, respectively (Fleet and Liu, 2007; Kim et al., 2016). The split bands at approximately 560 and 600 cm^{-1} are attributed to υ4 PO_4^{3-} vibration. In enamel crystals, carbonate (CO_3^{2-}) can substitute at two anionic sites in the hydroxyapatite lattice, namely the PO_4^{3-} position (B-type carbonated apatite) and OH^- position (A-type carbonated apatite) (Teruel Jde et al., 2015). For each group, a single weak absorption band at 1547 cm^{-1} (A-type), two overlapping bands at 1452 and 1411 cm^{-1} (B-type), and a vibration band of υ2 CO_3^{2-} at approximately 870 cm^{-1} were observed (Fleet and Liu, 2007; Kim et al., 2016). Compared with sound enamel, the υ3 PO_4^{3-} peak was significantly blue shifted from 981 to 1004 cm^{-1} in demineralized enamel. After 2 weeks of remineralization treatment, the υ3 PO_4^{3-} peak in Group 1 and Group 2 remained largely unchanged and no shift, in Group 3, it split up into 1011 and 983 cm^{-1}. However, the υ3 PO_4^{3-} peak in Group 4 showed a slightly red-shift to 996 cm^{-1}. The peaks at 1673 and 1532 cm^{-1} were assigned to the amide I and amide II vibrational models of protein. It is worth noting that the amide peaks were significantly enhanced in Group 4, in particular, strong absorption bands at 1581 and 1650 cm^{-1}.

The type of regenerated crystals on the enamel surface was investigated through XRD. As described in Fig. 5b, the diffraction peaks of

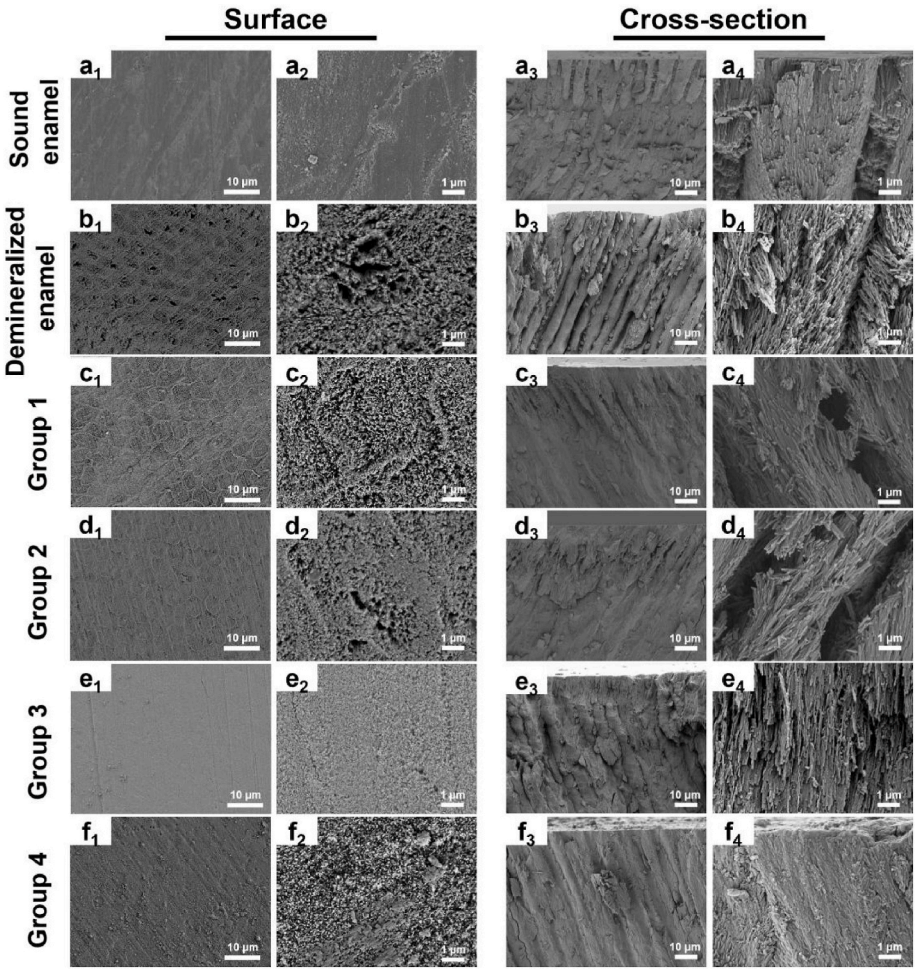

Fig. 4. SEM images taken at baseline, after 6-day demineralization and after 2-week remineralization treatments. (a_1-a_4) Images of sound enamel at baseline show a smooth and flat enamel surface, with the intact rods and inter-rods on cross sections. (b_1-b_4) Images of demineralized enamel before treatment show a 'fish scales' surface and a porous and disordered microstructure. (c_1-c_4) Images of Group 1 and (d_1-d_4) Group 2 after 2-week treatment, still existed a demineralized morphology with a pronounced crystal gaps. (e_1-e_4) Images of Group 3 show an inferior remineralization effect with the minerals partially deposited and the interstitial spaces among enamel crystals are detectable; whilst (f_1-f_4) images of Group 4 show a repaired enamel structures with the previously exposed interstitial spaces densely restored by new minerals. (a_2, b_2, c_2, d_2, e_2, and f_2) Corresponding high-magnification images of surface. (a_4, b_4, c_4, d_4, e_4, and f_4) Corresponding high-magnification images of cross sections.

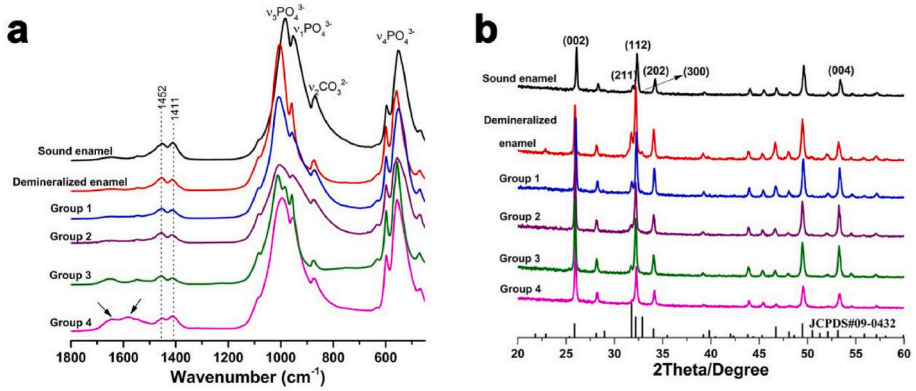

Fig. 5. Chemical properties of enamel surface in each group. (a) ATR-FTIR spectra, (b) XRD patterns.

(002), (211), (112), (300), and (202) at $2\theta = 25.8$, 31.8, 32.2, 32.8, and 34.1°, respectively, are characteristic of pure HAP (Fang et al., 2021). The diffraction peaks of sound enamel, demineralized enamel, and remineralized enamel in Group 1, 2, 3, and 4 were corresponded well to the peaks for standardized HAP diffraction pattern (JCPDS#09–0432), implying an identically organized crystallographic structure at the macroscopic level. The XRD pattern indicates that the mineral deposits on enamel surfaces in each group was mostly HAP, although there were some differences in spectra among the samples. Compared with sound enamel, the crystal plane of (211) was disappeared in the Group 4.

3.5. Mechanical properties

The mechanical properties of enamel samples from each group were examined by nanoindentation testing (Fig. 6). The load-displacement curves showed that the total indentation depth of demineralized enamel (nearly 1.5 μm) was much deeper than sound enamel (approximately 0.4 μm), and its depth was sequentially decreased in Group 1, 2, 3, and 4 (Fig. 6A). The hardness (H) and elastic modulus (Er) were further calculated (Fig. 6B). The sound enamel samples exhibited optimal mechanical performance, with an H value of 6.13 ± 0.77 GPa and an Er value of 112.08 ± 10.42 GPa. However, after 6 days of demineralization, the mechanical properties of the enamel were significantly weakened, with H of 0.29 ± 0.19 GPa and Er of 10.77 ± 5.30 GPa. After 2 weeks of remineralization, Group 1 and 2 provided little improvement in the mechanical strength, with H of 1.35 ± 0.36 and 1.63 ± 0.28 GPa, and Er of 22.57 ± 4.09 and 39.39 ± 4.89 GPa, respectively. In Group 3, the mechanical properties were somewhat recovered, as reflected by the increase of H and Er to 1.86 ± 0.31 and 46.60 ± 7.18 GPa, respectively. In contrast, although the mechanical strength remained weaker than that of sound enamel, the AFCP/HPMC film (Group 4) treatment resulted in the best mechanical enhancement ($P < 0.05$), with H and Er values of 2.69 ± 0.70 and 68.83 ± 12.72 GPa, respectively. The AFCP/HPMC film treatment greatly induced restoration of demineralized enamel in mechanical properties within a short time (2 weeks).

4. Discussions

The human enamel is mostly composed of non-stoichiometric HAP (Robinson et al., 2000). Different elemental substitutions can exist within the apatite, for example, the carbonate (CO_3^{2-}) ions can substitute the binding site of PO_4^{3-} and OH^- ions within the biological hydroxyapatite's crystal lattice (Fleet and Liu, 2007; Teruel Jde et al., 2015). In addition, enamel crystals contain many trace elements such as Mg, Na, Cl, and F (La Fontaine et al., 2016; Teruel Jde et al., 2015). Enamel caries can be almost viewed as a chemical process, in essence, an imbalance of the re- and demineralization equilibrium favoring demineralization on tooth surface. The remineralization is a dynamic process, it involves calcium and phosphate ions from external source are deposited into the crystal voids in a demineralized tooth tissue, exceeding the rate at which crystals are dissolved; this results in a net mineral gain. The initial stage of caries development occurs at the atomic level before it can be visualized as demineralization and asymptomatic (Selwitz et al., 2007). It has been reported that incipient enamel caries lessions can be reversed by the application of non-invasive techniques, such as biomimetic mineralization. The key to managing early enamel carious lesions is to provide a local ion-rich micro-environment that can promote biomineralization. In the previous study, we discovered that the mineralizing film consisting of HPMC and AFCP nanoparticles can effectively inhibit the formation of enamel WSLs (Zhang et al., 2021). Therefore, this study focused on the therapy effects of AFCP/HPMC film on enamel ACL, with the aid of Micro-CT, SEM-EDX, ATR-FTIR, XRD, and nanoindentation methods.

Calcium phosphate ions are unable to be combined with fluoride ions in dental products since fluorine have the tendency to react with calcium ions and create insoluble products such as calcium fluoride (CaF_2), which results in loss of bioavailable fluoride ions (Shen et al., 2021; Cochrane et al., 2010; Meyer et al., 2018). To overcome this challenge, the chelating agent was used to stabilize the free calcium, phosphate and fluorions to obtain amorphous fluorinated calcium phosphate (AFCP) nanoparticles, which were developed to provide bioavailable and stable calcium, phosphate and fluorion. As seen in Fig. 2B and C, both the FTIR spectrum and the XRD pattern indicate that the AFCP nanoparticles are amorphous (Combes and Rey, 2010). The size of the AFCP nanoparticles provides a possibility of remineralization of demineralized enamel via penetrating into crystal gaps (Fig. 2A). Additionally, the AFCP/HPMC film was non-cytotoxic even at a high concentration of 8 mg mL^{-1} (Figs. S1a–d), and was judged to be a non-irritating to oral mucosa according to YY/T 0127.13–2018 (Figs. S1e–h). Therefore, the AFCP/HPMC film with excellent biocompatibility will enrich our clinical applications (Mokabber et al., 2020).

Micro-CT is an accurate, advanced technique that can provide three-dimensional information, and quantify enamel lesion depth and mineral content (Schwass et al., 2009; Efeoglu et al., 2005). Further, the nanoindentation test is recognized as one of the most sensitive methods for investigating enamel mechanical properties (Angker and Swain, 2006). The AFCP/HPMC film group in this study displayed not only the highest remineralization rate with the least lesion depth and mineral loss, but also the best restoration of mechanical properties (Figs. 3 and 6). Without special treatment, the demineralized enamel lesions were still clearly visible after 2-week pH cycling in Group 1 (Fig. 4$c_{1\text{-}4}$). These observations indicate that natural remineralization is restricted by salivary calcium and phosphate ion concentrations, resulting in a very low efficiency. When using the AFCP/HPMC film, the microstructural integrity of demineralized enamel was greatly improved as the voids caused by acid challenge were densely re-deposited with minerals (Fig. 4$f_{1\text{-}4}$). It is most likely that these intermediate structures are a result of nanosized AFCP particles that are easily able to penetrate into the interprismatic zones. The AFCP nanoprecursors serve as an exogenous supply of Ca^{2+}, PO_4^{3-}, and F^- ions. The newly formed minerals could be HAP, fluorapatite (FAP), as well as CaF_2, therefore, EDX analysis (Fig. S2) showed a higher Ca/F ratio in the AFCP/HPMC film group than the controls (Dogan et al., 2018).

Based on our experimental results, the null hypotheses that AFCP/

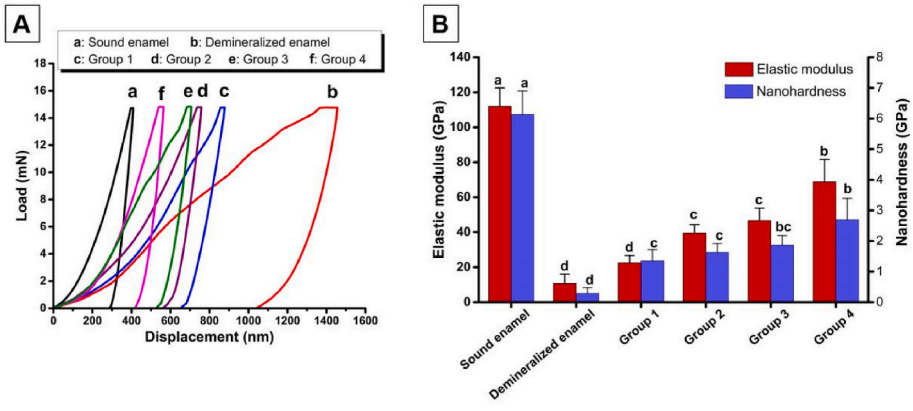

Fig. 6. Typical load–displacement curves (A) and calculated nanohardness and elastic modulus (B) of different enamel surfaces. The data are represented as means ± SD. Bars showing the different letters denote statistical significance ($p < 0.05$), according to Tukey's HSD post hoc test.

HPMC film neither can promote enamel ACL remineralization nor restore enamel ACL mechanical performance can be totally rejected. When enamel is demineralized, the

defects and gaps of enamel might become nucleation sites for mineral ions (Yin et al., 2009). In this situation, calcium and phosphate ions could infiltrate into enamel inter-crystal gaps and deposited there (Fig. 4). Fluoride ions (F^-) can substitute randomly for OH^- or CO_3^{2-} ions of the HAP to form FAP on and in the enamel, which is more resistant to acid challenge. The AFCP/HPMC film can gradually release of Ca^{2+}, PO_4^{3-}, and F^- ions, which generates local supersaturation and triggers the remineralization of tooth hard tissues. The AFCP/HPMC film not only supplies the ions but also prevents their rapid aggregation and spontaneous transformation at the surface of lesions, which allows greater penetration of Ca^{2+}, PO_4^{3-}, and F^- ions into the gaps to accelerate internal crystal growth and promote formation of a dense remineralized layer. As shown in Fig. 5, the ATR-FTIR spectra of the amide region in AFCP/HPMC film treatment group coincide with the bands of AFCP nanoparticles (Zhang et al., 2021), and the XRD pattern indicated that the newly formed crystals on the enamel surface were low crystallinity (Fang et al., 2021). The results of ATR-FTIR and XRD suggest that the solid AFCP nanoparticles in the HPMC film might be directly attached to the enamel surface for in-situ nucleation, and converted to HAP by solid-solid phase transformation. Hence, the enamel caries lesion might be reversed by AFCP/HPMC film due to mineral content increase and mechanical performance recover.

The fast crystallization-deposition of minerals on the surface zone of enamel caries often acts as a barrier to prevent minerals from entering the lesion, which reduces the efficacy of subsurface remineralization (Philip, 2019; Xu et al., 2022). This might be the reason that fluoride mediated salivary remineralization seems to be restricted to the outer layer about 30 μm of the tooth surface (Schmidlin et al., 2016). Currently, CPP-ACP with fluoride have been widely studied to manage dental caries (Sleibi et al., 2019). So, this study we used Tooth Mousse Plus as a positive control. The AFCP/HPMC film exhibited a better therapeutic efficacy for enamel ACL than Tooth Mousse Plus in this study. The reasons for this may be manifold. First, the mineral ions released from AFCP/HPMC film were more stable and sustained at relatively high levels (Zhang et al., 2021). Second, the bioactivity of AFCP nanoprecursors in dried HPMC film can be preserved in a stable, solid form, yet the fluoride in Tooth Mousse Plus is simple admixture with CPP-ACP.(Sleibi et al., 2019). Additionally, the water-soluble features of HPMC may provide advantages for releasing AFCP nanoparticles. The AFCP/HPMC film applied to the enamel surface in oral cavity will gradually turn into hydrogel state, resulting in biomimetic mineralization. Therefore, AFCP/HPMC film might be applied onto tooth surface during night sleep for 6–8 h.

5. Conclusion

The AFCP/HPMC film not only could reduce lesion depth and mineral loss of the enamel ACL, promote its rapid remineralization, but also greatly improve its mechanical properties when it was challenge by pH cycling. Furthermore, the AFCP/HPMC film possessed excellent biocompatibility without any cytotoxicity. Therefore, the AFCP/HPMC film might provide a promising therapy for reversing incipient enamel caries via inhibiting enamel demineralization and promoting enamel remineralization.

CRediT authorship contribution statement

Zhixin Zhang: Writing – original draft, Visualization, Investigation, Data curation. **Zihan Cui:** Writing – original draft, Visualization, Data curation. **Jianping Zhang:** Data curation. **Haiyan Zheng:** Data curation. **Zihuai Zhou:** Methodology. **Zhifang Wu:** Writing – review & editing. **Zhe Wang:** Writing – review & editing, Conceptualization. **Baiping Fu:** Writing – review & editing, Supervision, Funding acquisition, Conceptualization.

Declaration of competing interest

The authors declare that they have no known competing financial interests or personal relationships that could have appeared to influence the work reported in this paper.

Data availability

The authors do not have permission to share data.

Acknowledgements

This study was supported by the National Natural Science Foundation of China (NO. 81970982), and the Key Research and Development Plan Projects of Zhejiang Province (No. 2020C03037).

Appendix A. Supplementary data

Supplementary data to this article can be found online at https://doi.org/10.1016/j.jmbbm.2024.106408.

References

Abou Neel, E.A., Aljabo, A., Strange, A., Ibrahim, S., Coathup, M., Young, A.M., Bozec, L., Mudera, V., 2016. Demineralization-remineralization dynamics in teeth and bone. Int. J. Nanomed. 11, 4743–4763. https://doi.org/10.2147/IJN.S107624.

Angker, L., Swain, M.V., 2006. Nanoindentation: application to dental hard tissue investigations. J. Mater. Res. 21 (8), 1893–1905. https://doi.org/10.1557/jmr.2006.0257.

Baghel, S., Cathcart, H., O'Reilly, N.J., 2016. Polymeric amorphous solid dispersions: a review of amorphization, crystallization, stabilization, solid-state characterization, and aqueous solubilization of biopharmaceutical classification system class II drugs. J. Pharm. Sci. 105 (9), 2527–2544. https://doi.org/10.1016/j.xphs.2015.10.008.

Balhaddad, A.A., Kansara, A.A., Hidan, D., Weir, M.D., Xu, H.H.K., Melo, M.A.S., 2018. Toward dental caries: exploring nanoparticle-based platforms and calcium phosphate compounds for dental restorative materials. Bioact. Mater. 4 (1), 43–55. https://doi.org/10.1016/j.bioactmat.2018.12.002.

Bayne, S.C., Ferracane, J.L., Marshall, G.W., Marshall, S.J., van Noort, R., 2019. The evolution of dental materials over the past century: silver and gold to tooth color and beyond. J. Dent. Res. 98 (3), 257–265. https://doi.org/10.1177/0022034518822808.

Benson, P.E., Parkin, N., Dyer, F., Millett, D.T., Germain, P., 2019. Fluorides for preventing early tooth decay (demineralised lesions) during fixed brace treatment. Cochrane Database Syst. Rev. 2019 (11), CD003809 https://doi.org/10.1002/14651858.CD003809.

Cantaert, B., Beniash, E., Meldrum, F.C., 2013. The role of poly(aspartic acid) in the precipitation of calcium phosphate in confinement. J. Mater. Chem. B 1 (48). https://doi.org/10.1039/C3TB21296C, 10.1039/C3TB21296C.

Cochrane, N.J., Saranathan, S., Cai, F., Cross, K.J., Reynolds, E.C., 2008. Enamel subsurface lesion remineralisation with casein phosphopeptide stabilised solutions of calcium, phosphate and fluoride. Caries Res. 42 (2), 88–97. https://doi.org/10.1159/000113161.

Cochrane, N.J., Cai, F., Huq, N.L., Burrow, M.F., Reynolds, E.C., 2010. New approaches to enhanced remineralization of tooth enamel. J. Dent. Res. 89 (11), 1187–1197. https://doi.org/10.1177/0022034510376046.

Combes, C., Rey, C., 2010. Amorphous calcium phosphates: synthesis, properties and uses in biomaterials. Acta Biomater. 6 (9), 3362–3378. https://doi.org/10.1016/j.actbio.2010.02.017.

Cramer, N.B., Stansbury, J.W., Bowman, C.N., 2011. Recent advances and developments in composite dental restorative materials. J. Dent. Res. 90 (4), 402–416. https://doi.org/10.1177/0022034510381263.

Demarco, F.F., Corrêa, M.B., Cenci, M.S., Moraes, R.R., Opdam, N.J., 2012. Longevity of posterior composite restorations: not only a matter of materials. Dent. Mater. 28 (1), 87–101. https://doi.org/10.1016/j.dental.2011.09.003.

DeRocher, K.A., Smeets, P.J.M., Goodge, B.H., Zachman, M.J., Balachandran, P.V., Stegbauer, L., Cohen, M.J., Gordon, L.M., Rondinelli, J.M., Kourkoutis, L.F., Joester, D., 2020. Chemical gradients in human enamel crystallites. Nature 583 (7814), 66–71. https://doi.org/10.1038/s41586-020-2433-3.

Dogan, S., Fong, H., Yucesoy, D.T., Cousin, T., Gresswell, C., Dag, S., Huang, G., Sarikaya, M., 2018. Biomimetic tooth repair: amelogenin-derived peptide enables in vitro remineralization of human enamel. ACS Biomater. Sci. Eng. 4 (5), 1788–1796. https://doi.org/10.1021/acsbiomaterials.7b00959.

Dorozhkin, S.V., 2010. Amorphous calcium (ortho)phosphates. Acta Biomater. 6 (12), 4457–4475. https://doi.org/10.1016/j.actbio.2010.06.031.

Eanes, E.D., Termine, J.D., Nylen, M.U., 1973. An electron microscopic study of the formation of amorphous calcium phosphate and its transformation to crystalline apatite. Calcif. Tissue Res. 12 (2), 143–158. https://doi.org/10.1007/BF02013730.
Efeoglu, N., Wood, D., Efeoglu, C., 2005. Microcomputerised tomography evaluation of 10% carbamide peroxide applied to enamel. J. Dent. 33 (7), 561–567. https://doi.org/10.1016/j.jdent.2004.12.001.
El Gezawi, M., Wölfle, U.C., Haridy, R., Fliefel, R., Kaisarly, D., 2019. Remineralization, regeneration, and repair of natural tooth structure: influences on the future of restorative dentistry practice. ACS Biomater. Sci. Eng. 5 (10), 4899–4919. https://doi.org/10.1021/acsbiomaterials.9b00591.
Fang, Z., Guo, M., Zhou, Q., Li, Q., Wong, H.M., Cao, C.Y., 2021. Enamel-like tissue regeneration by using biomimetic enamel matrix proteins. Int. J. Biol. Macromol. 183, 2131–2141. https://doi.org/10.1016/j.ijbiomac.2021.06.028.
Fleet, M.E., Liu, X., 2007. Coupled substitution of type A and B carbonate in sodium-bearing apatite. Biomaterials 28 (6), 916–926. https://doi.org/10.1016/j.biomaterials.2006.11.003.
Gauthier, R., Aboulleil, H., Chenal, J.M., Chevalier, J., Colon, P., Grosgogeat, B., 2021. Consideration of dental tissues and composite mechanical properties in secondary caries development: a critical review. J. Adhes. Dent. 23 (4), 297–308. https://doi.org/10.3290/j.jad.b1649941.
He, J., Yang, J., Li, M., Li, Y., Pang, Y., Deng, J., Zhang, X., Liu, W., 2022. Polyzwitterion manipulates remineralization and antibiofilm functions against dental demineralization. ACS Nano 16 (2), 3119–3134. https://doi.org/10.1021/acsnano.1c10812.
Kim, I.H., Son, J.S., Min, B.K., Kim, Y.K., Kim, K.H., Kwon, T.Y., 2016. A simple, sensitive and non-destructive technique for characterizing bovine dental enamel erosion: attenuated total reflection Fourier transform infrared spectroscopy. Int. J. Oral Sci. 8 (1), 54–60. https://doi.org/10.1038/ijos.2015.58.
La Fontaine, A., Zavgorodniy, A., Liu, H., Zheng, R., Swain, M., Cairney, J., 2016. Atomic-scale compositional mapping reveals Mg-rich amorphous calcium phosphate in human dental enamel. Sci. Adv. 2 (9), e1601145 https://doi.org/10.1126/sciadv.1601145.
Lacruz, R.S., Habelitz, S., Wright, J.T., Paine, M.L., 2017. Dental enamel formation and implications for oral health and disease. Physiol. Rev. 97 (3), 939–993. https://doi.org/10.1152/physrev.00030.2016.
Li, N., Cui, W., Cong, P., Tang, J., Guan, Y., Huang, C., Liu, Y., Yu, C., Yang, R., Zhang, X., 2021. Biomimetic inorganic-organic hybrid nanoparticles from magnesium-substituted amorphous calcium phosphate clusters and polyacrylic acid molecules. Bioact. Mater. 6 (8), 2303–2314. https://doi.org/10.1016/j.bioactmat.2021.01.005.
Lippert, F., Juthani, K., 2015. Fluoride dose-response of human and bovine enamel artificial caries lesions under pH-cycling conditions. Clin. Oral Invest. 19 (8), 1947–1954. https://doi.org/10.1007/s00784-015-1436-1.
Lyaruu, D.M., Medina, J.F., Sarvide, S., Bervoets, T.J., Everts, V., Denbesten, P., Smith, C. E., Bronckers, A.L., 2014. Barrier formation: potential molecular mechanism of enamel fluorosis. J. Dent. Res. 93 (1), 96–102. https://doi.org/10.1177/0022034513510944.
Meyer, F., Amaechi, B.T., Fabritius, H.O., Enax, J., 2018. Overview of calcium phosphates used in biomimetic oral care. Open Dent. J. 12, 406–423. https://doi.org/10.2174/1874210601812010406.
Mokabber, T., Cao, H.T., Norouzi, N., van Rijn, P., Pei, Y.T., 2020. Antimicrobial electrodeposited silver-containing calcium phosphate coatings. ACS Appl. Mater. Interfaces 12 (5), 5531–5541. https://doi.org/10.1021/acsami.9b20158.
Oliver, W.C., Pharr, G.M., 2004. Measurement of hardness and elastic modulus by instrumented indentation: advances in understanding and refinements to methodology. J. Mater. Res. 19, 3–20.
Philip, N., 2019. State of the art enamel remineralization systems: the next frontier in caries management. Caries Res. 53 (3), 284–295. https://doi.org/10.1159/000493031.
Pitts, N.B., Zero, D.T., Marsh, P.D., Ekstrand, K., Weintraub, J.A., Ramos-Gomez, F., Tagami, J., Twetman, S., Tsakos, G., Ismail, A., 2017. Dental caries. Nat. Rev. Dis. Prim. 3, 17030 https://doi.org/10.1038/nrdp.2017.30.
Rabadjieva, D., Gergulova, R., Titorenkova, R., Tepavitcharova, S., Dyulgerova, E., Balarew, C., Petrov, O., 2010. Biomimetic transformations of amorphous calcium phosphate: kinetic and thermodynamic studies. J. Mater. Sci. Mater. Med. 21 (9), 2501–2509. https://doi.org/10.1007/s10856-010-4103-8.
Reynolds, E.C., Cai, F., Shen, P., Walker, G.D., 2003. Retention in plaque and remineralization of enamel lesions by various forms of calcium in a mouthrinse or sugar-free chewing gum. J. Dent. Res. 82 (3), 206–211. https://doi.org/10.1177/154405910308200311.
Robinson, C., Shore, R.C., Brookes, S.J., Strafford, S., Wood, S.R., Kirkham, J., 2000. The chemistry of enamel caries. Crit. Rev. Oral Biol. Med. 11 (4), 481–495. https://doi.org/10.1177/10454411000110040601.
Ruan, Q., Moradian-Oldak, J., 2015. Amelogenin and enamel biomimetics. J. Mater. Chem. B 3, 3112–3129. https://doi.org/10.1039/C5TB00163C.
Sa, Y., Liang, S., Ma, X., Lu, S., Wang, Z., Jiang, T., Wang, Y., 2014. Compositional, structural and mechanical comparisons of normal enamel and hypomaturation enamel. Acta Biomater. 10 (12), 5169–5177. https://doi.org/10.1016/j.actbio.2014.08.023.
Schmidlin, P., Zobrist, K., Attin, T., Wegehaupt, F., 2016. In vitro re-hardening of artificial enamel caries lesions using enamel matrix proteins or self-assembling peptides. J. Appl. Oral Sci. 24 (1), 31–36. https://doi.org/10.1590/1678-775720150352.
Schwass, D.R., Swain, M.V., Purton, D.G., Leichter, J.W., 2009. A system of calibrating microtomography for use in caries research. Caries Res. 43 (4), 314–321. https://doi.org/10.1159/000226230.
Selwitz, R.H., Ismail, A.I., Pitts, N.B., 2007. Dental caries. Lancet 369 (9555), 51–59. https://doi.org/10.1016/S0140-6736(07)60031-2.
Shen, P., Walker, G.D., Yuan, Y., Reynolds, C., Stanton, D.P., Fernando, J.R., Reynolds, E. C., 2018. Importance of bioavailable calcium in fluoride dentifrices for enamel remineralization. J. Dent. 78, 59–64. https://doi.org/10.1016/j.jdent.2018.08.005.
Shen, P., Fernando, J.R., Yuan, Y., Walker, G.D., Reynolds, C., Reynolds, E.C., 2021. Bioavailable fluoride in calcium-containing dentifrices. Sci. Rep. 11 (1), 146. https://doi.org/10.1038/s41598-020-80503-x.
Siepmann, J., Peppas, N.A., 2001. Modeling of drug release from delivery systems based on hydroxypropyl methylcellulose (HPMC). Adv. Drug Deliv. Rev. 48 (2–3), 139–157. https://doi.org/10.1016/s0169-409x(01)00112-0.
Sleibi, A., Tappuni, A.R., Karpukhina, N.G., Hill, R.G., Baysan, A., 2019. A comparative evaluation of ion release characteristics of three different dental varnishes containing fluoride either with CPP-ACP or bioactive glass. Dent. Mater. 35 (12), 1695–1705. https://doi.org/10.1016/j.dental.2019.08.113.69.
Stewart, C.A., Finer, Y., 2019. Biostable, antidegradative and antimicrobial restorative systems based on host-biomaterials and microbial interactions. Dent. Mater. 35 (1), 36–52. https://doi.org/10.1016/j.dental.2018.09.013.
Sun, L., Liang, S., Sa, Y., Wang, Z., Ma, X., Jiang, T., Wang, Y., 2011. Surface alteration of human tooth enamel subjected to acidic and neutral 30% hydrogen peroxide. J. Dent. 39 (10), 686–692. https://doi.org/10.1016/j.jdent.2011.07.011.
Teruel Jde, D., Alcolea, A., Hernández, A., Ruiz, A.J., 2015. Comparison of chemical composition of enamel and dentine in human, bovine, porcine and ovine teeth. Arch. Oral Biol. 60 (5), 768–775. https://doi.org/10.1016/j.archoralbio.2015.01.014.
Tran, P.H., Tran, T.T., Park, J.B., Lee, B.J., 2011. Controlled release systems containing solid dispersions: strategies and mechanisms. Pharm. Res. (N. Y.) 28 (10), 2353–2378. https://doi.org/10.1007/s11095-011-0449-y.
Wang, J., Liu, Z., Ren, B., Wang, Q., Wu, J., Yang, N., Sui, X., Li, L., Li, M., Zhang, X., Li, X., Wang, B., 2021. Biomimetic mineralisation systems for in situ enamel restoration inspired by amelogenesis. J. Mater. Sci. Mater. Med. 32 (9), 115. https://doi.org/10.1007/s10856-021-06583-x.
Xiao, Z., Que, K., Wang, H., An, R., Chen, Z., Qiu, Z., Lin, M., Song, J., Yang, J., Lu, D., Shen, M., Guan, B., Wang, Y., Deng, X., Yang, X., Cai, Q., Deng, J., Ma, L., Zhang, X., Zhang, X., 2017. Rapid biomimetic remineralization of the demineralized enamel surface using nano-particles of amorphous calcium phosphate guided by chimaeric peptides. Dent. Mater. 33 (11), 1217–1228. https://doi.org/10.1016/j.dental.2017.07.015.
Xu, J., Shi, H., Luo, J., Yao, H., Wang, P., Li, Z., Wei, J., 2022. Advanced materials for enamel remineralization. Front. Bioeng. Biotechnol. 10, 985881 https://doi.org/10.3389/fbioe.2022.985881.
Yang, Y., Lv, X.P., Shi, W., Li, J.Y., Li, D.X., Zhou, X.D., Zhang, L.L., 2014. 8DSS-promoted remineralization of initial enamel caries in vitro. J. Dent. Res. 93 (5), 520–524. https://doi.org/10.1177/0022034514522815.
Yin, Y., Yun, S., Fang, J., Chen, H., 2009. Chemical regeneration of human tooth enamel under near-physiological conditions. Chem. Commun. 2, 5892–5894. https://doi.org/10.1039/b911407.
Yu, L., Martin, I.J., Kasi, R.M., Wei, M., 2018. Enhanced intrafibrillar mineralization of collagen fibrils induced by brushlike polymers. ACS Appl. Mater. Interfaces 10 (34), 28440–28449. https://doi.org/10.1021/acsami.8b10234.
Yu, O.Y., Mei, M.L., Zhao, I.S., Li, Q.L., Lo, E.C., Chu, C.H., 2018. Remineralisation of enamel with silver diamine fluoride and sodium fluoride. Dent. Mater. 34 (12), e344–e352. https://doi.org/10.1016/j.dental.2018.10.007.
Zhang, L., Weir, M.D., Chow, L.C., Antonucci, J.M., Chen, J., Xu, H.H., 2016. Novel rechargeable calcium phosphate dental nanocomposite. Dent. Mater. 32 (2), 285–293. https://doi.org/10.1016/j.dental.2015.11.015.
Zhang, Z., Shi, Y., Zheng, H., Zhou, Z., Wu, Z., Shen, D., Wang, Y., Zhang, Y., Wang, Z., Fu, B., 2021. A hydroxypropyl methylcellulose film loaded with AFCP nanoparticles for inhibiting formation of enamel white spot lesions. Int. J. Nanomed. 16, 7623–7637. https://doi.org/10.2147/IJN.S335549.